FAST DETERMINATION OF HELIOSTAT SHAPE AND ORIENTATION BY EDGE DETECTION AND PHOTOGRAMMETRY

Marc Röger, Christof Prahl, Steffen Ulmer

German Aerospace Center (DLR), Institute of Technical Thermodynamics, Solar Research,
Plataforma Solar de Almería, 04200 Tabernas, Spain
phone: +34-950387935, fax: +34-950365313, email: marc.roeger@dlr.de

Abstract

Heliostats of central receiver solar power plants reach dimensions up to 150 m^2 with focal lengths up to 1000 m. Their optical properties and tracking accuracy have great influence on the power plant efficiency and need to be monitored both at plant start up and during operation. Up to now, there are few efficient and fast measurement techniques to access the heliostat properties. Flux density measurements and close-range photogrammetry are possible approaches, yet they do not fulfill the requirement to be accurate, inexpensive and fast at the same time. In this paper, we present a non-contact measurement principle, which uses edge detection to extract the heliostat and facet vertices. This information is used to calculate the surface normals. Furthermore, the corners can replace retroreflective targets generally used in close-range photogrammetry, thus enabling a fast and completely automatic evaluation of the three-dimensional heliostat structure. The pictures are provided by a digital camera which is mounted on a pan tilt head on top of the central receiver tower, offering visibility to all heliostats and allowing the automated qualification of whole heliostat fields in a short period of time. It is shown that measurement uncertainties in heliostat orientation for the investigated heliostat are below 4 mrad in 80% of the relevant heliostat positions. Heliostat orientation is available within three minutes. Photogrammetric measurements based on edge detection at a 40-m^2 CESA-1 heliostat at the Plataforma Solar de Almerìa (PSA) exhibit an accuracy of 1.6 mrad for a single-facet normal vector with the results being available within 30 minutes. The reduced measurement time allows the economic characterization of entire heliostat fields. The lower accuracy compared to manual photogrammetry with retroreflective targets is still sufficient to detect facet misalignments in existing heliostat fields.

Keywords: edge detection, photogrammetry, heliostat shape, heliostat orientation, solar tower, digital imaging

1 Introduction

Solar thermal power plants will play a key role in future energy supply. Point and line concentrating systems are two different ways to use the thermal energy of sunlight to generate electricity. A major cost factor of central receiver systems (CRS) are the heliostats, consisting of an array of almost flat mirror facets, which are tracked biaxially to focus the sunlight onto the receiver located on top of the central tower. The shape of the mirror surface and the tracking accuracy affect directly the plant performance. Heliostats are usually tracked either with suns sensors or angle transmitters. Since future CRS heliostat fields will consist of up to several thousand heliostats, there is need for a reliable, cost-effective and fast measurement method to verify heliostat quality and monitor heliostat tracking independently of their tracking sensor.

Three different non-contact methods exist up to now, which provide information about the mirror shape and/or the tracking of one single heliostat. One approach is to take pictures of the heliostat beam image. Knowing the position of the sun, this permits access to the heliostat surface normal and integral optical properties. However, it does not offer detailed information about the heliostat structure and slope errors. In these fields, the second and third method, close-range photogrammetry [1] and deflectometry[2], provide very accurate and highly resolved information. Each of these methods has its own field of application, but what we were looking for was a cost-effective, fast and fully automatic characterization tool while keeping the loss of accuracy to a minimum.

The approach of this paper is to automatically detect the corners of the mirror facets in digital images. The determination and assignment of these corners was implemented combining several standard images processing techniques. The stability and accuracy of this method directly affects the subsequent calculations. With the detected points, the heliostat orientation is calculated. Moreover, the photogrammetric investigation of heliostats was simplified by replacing the retroreflective targets with the automatically detected corner points, which is so far a time-consuming procedure.

The following section gives a detailed description of the corner detection procedure and an estimation of its precision. Sections 3 deals with the calculation of the heliostat orientation and section 4 describes the modification of the photogrammetric evaluation. Both sections are completed by a discussion of their accuracy

compared to previous approaches. The paper completes with an outlook to further projects and possible improvements of the developed method.

2 Edge Detection

Most heliostats of solar thermal power plants feature a regular structure, consisting of rectangular mirror facets. The facet corner positions in a digital image can be exploited to establish the actual direction of the surface normal of the corresponding facets and further information about the heliostats optical properties. The automatic computation and assignment of the facet corners is described in the following section. The reliability of this method depends on the quality of the images and, to a minor degree, on the weather conditions and the heliostat design. Generally, the corners can be evaluated with a standard deviation smaller than two pixels.

2.1 Approach

The edge detection procedure was developed with the Matlab Image Processing Toolbox [3]. The pictures of the heliostats were taken with a Nikon D2Xs digital camera (12 megapixels) and a Sigma zoom lens with 170-500 mm focal length. The studied objects were the 40-m^2 CASA heliostats of the CESA-1 test facility at the PSA (see Fig. 1). To obtain a good view over the whole field and a uniform luminance within the mirror facets, the pictures were taken from the top of the central tower.

The first step in the edge detection procedure is to select the RGB plane with the best contrast, which is in general the blue channel. The resulting grayscale image is transformed to a binary image using standard thresholding. Based on that data, the heliostat is identified so that a region of interest (ROI) can be set. A more elaborate thresholding method is applied to that ROI until the single facets of the heliostat can be distinguished. Disturbing objects like facets of other heliostats are removed by morphological opening.

The segmentation is finished when all facets are identified and the structure of the heliostat is available as a binary image (mask). An edge filter using the Sobel method is applied to the initial grayscale image. The multiplication of the mask with the edge image results in a binary image, in which only the edges of one facet are visible. The Hough transformation is used to calculate the linear equation parameters of each mirror edge. To avoid singularities for vertical lines, the normal representation is chosen. A straight line is then characterized by its distance from the origin ρ and the angle γ which it encloses with the horizontal axis of the image. With these parameters, it is possible intersect the edges and to access the four corners of each facet.

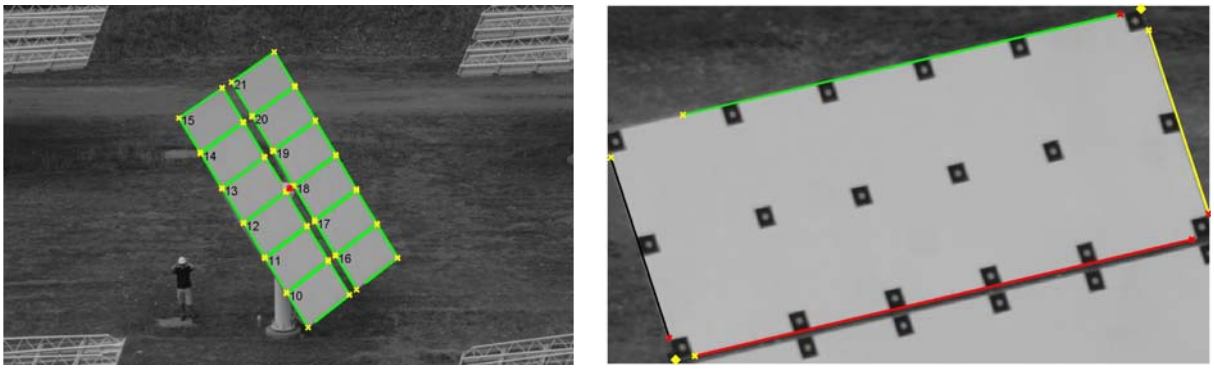

Figure 1. 40-m^2 CASA heliostat with detected edges (green), corners (yellow) and gearbox (red), left. Single facet with detected items and additional retroreflective targets, right

2.2 Validation and Error Estimation

Since the corners are calculated via the intersection of the mirror edges, the method can be very accurate reaching subpixel precision. Yet, false detection of the edges caused by limited resolution and noise makes it necessary to estimate the deviation of detected corners from their true position. The following error estimation is made under the assumption of negligible distortion. Subject to this simplification, opposite mirror edges are expected to be parallel. The angle deviation between opposite edges was used to access the errors of the corner coordinates in edge direction. In addition, the error rises further by the limited resolution of the Hough transformation $\Delta\rho$ and $\Delta\gamma$. Let dλ be the angle deviation between opposite edges $\vec{u}_\mathrm{i}$ and $\vec{u}_\mathrm{j}$, $\left|\vec{u}_\mathrm{i}\right|$ the length of the detected line segment, and $\left|\vec{u}_\mathrm{i,true}\right|$ being the actual distance between two intersection points. The error estimate for the corner coordinate in edge direction $\vec{u}_\mathrm{i}$ is:

$$d\vec{u}_i = 0.5 \cdot \Delta\rho \cdot \frac{\vec{u}_i}{|\vec{u}_i|} + \left(0.5 \cdot \Delta\gamma + d\lambda \cdot \frac{|\vec{u}_j|}{|\vec{u}_i| + |\vec{u}_j|} \right) \cdot \vec{u}_{i,true} \quad (1)$$

As mentioned above, this method tends to overestimate the actual deviations, especially for great values of azimuth and elevation and for heliostats close to the tower. However, the error estimates can be utilized to automatically detect outliers that are not used for photogrammetry and heliostat orientation.

To access the statistical properties of the corners calculated by the edge detection procedure, 20 pictures of the same heliostat were compared, while the position of the heliostat in the image was modified by moving the camera slightly. The averaged standard deviation of the detected corners was 1.2 pixels in x direction and 1.7 pixels in y direction.

3 Heliostat Orientation

3.1 Approach

The human eye can intuitively estimate the orientation of an object by interpreting all the information provided by the image, comprising of the angles, side ratios, perspective distortions, shadows, reflections, etc. In contrast, machine vision is usually capable to process only the geometric properties, such as angles and side ratios.

The approach to determine heliostat orientation presented in this paper uses only the corner points detected by edge detection. To achieve insensitivity to camera zoom and rotation around the optical axis, the ratios of facet side lengths Φ and the angles θ between observed edges are used (dimensionless quantities).

Fig. 2 left shows a 24-facet heliostat as seen by a camera located on top of the tower. The right figure shows a close-up of the left upper facet and the vectors and angles used to calculate the orientation. A parallel projection of a rectangle results in a parallelogram, whose opposing angles and side ratios of opposite edges are identical. Hence, a rectangle in parallel projection is defined unambiguously by one side ratio Φ and one angle θ. However, the process of imaging is better described by central projection. In this case, the angles and sides are usually differently distorted, leading to a planar quadrilateral. The perspective projection depends on the angle between line of sight and rectangle surface normal and the distance between camera and rectangle. The shape, but not the size, of a planar quadrilateral is sufficiently defined by the two side ratios Φ_1 and Φ_2 and two angles θ_1 and θ_2, shown in Fig. 2 left:

$$\theta_1 = \frac{\vec{a} \cdot \vec{b}}{|\vec{a}| \cdot |\vec{b}|} \quad (2) \qquad \theta_2 = \frac{-\vec{b} \cdot \vec{c}}{|\vec{b}| \cdot |\vec{c}|} \quad (3)$$

$$\phi_1 = \frac{b}{a} \quad (4); \qquad \phi_2 = \frac{c}{b} \quad (5)$$

Hence, the facet orientation relative to an observer can be calculated by measuring the two side ratios and angles when the position of the heliostat and camera are known precisely.

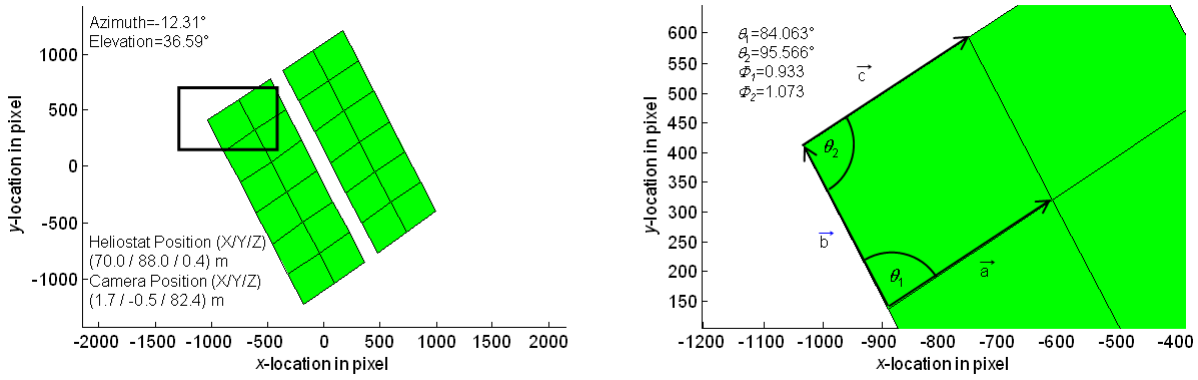

Figure 2. Heliostat as observed from the camera on tower top (left). Close-up of the upper left heliostat facet and the derived characteristic values (right). Details see Table 1

	Value
Camera Position ($X_0/Y_0/Z_0$) in m	(1.7 / -0.5 / 82.4)
Heliostat Position ($X_{Hel}/Y_{Hel}/Z_{Hel}$) in m	Hel 506: (30.0 / 88.0 / 0.4) Hel 514: (70.0 / 88.0 / 0.4)
Heliostat Azimuth / Elevation in deg	Fig. 2 and 3: -12.31° / 36.59°

Origin on tower front side; *x* direction: East; *y* direction: South; z direction: Height

Table 1. Detailed position / orientation data

3.2 Measurement Evaluation

The results of the edge detection (described in section 2) are corrected for lens distortion (internal orientation). Then the side ratios $\Phi_{i,meas}$ and angles $\theta_{i,meas}$ are determined for each facet. The external camera orientation can be calculated if the heliostat and camera location is known. In case the heliostat optical axis is not mapped at the image center, the camera pan and tilt are corrected accordingly. The rotation around the camera axis has no influence on the results.

The quantities $\Phi_{i,meas}$ and $\theta_{i,meas}$, calculated from measured vertices, are compared to $\Phi_{i,calc}(\alpha,\beta)$ and $\theta_{i,calc}(\alpha,\beta)$ which are calculated for a given heliostat azimuth α and elevation β by performing a central projection. By varying α and β, the difference between measured ($C_{i,meas}$) and calculated quantities ($C_{i,calc}$) is minimized, until the global maximum of χ is found:

$$\chi^{-1} = \sum_{i=1}^{4} \frac{\left[C_{i,meas} - C_{i,calc}(\alpha,\beta) \right]^2}{\sigma_i} \tag{6}$$

The corresponding α and β represent the orientation of the facet. An overview of the variables used in Eq. (6) is given in Table 2. The optimization is done by a genetic algorithm[4], followed by a simplex search method[5] to enhance accuracy, both implemented in Matlab.

Since the facet and heliostat center location change with heliostat azimuth and elevation, the camera is oriented a second time with the initially calculated azimuth and elevation, and subsequently an improved azimuth and elevation is calculated. The heliostat azimuth and elevation is calculated as the mean of all heliostat facets. Averaging over several pictures taken in quick succession minimizes statistical errors.

	Quantity C_i	Factor σ_i
1	Side ratio Φ_1	0.1
2	Side ratio Φ_2	0.1
3	Angle θ_1	1
4	Angle θ_2	1

Table 2. Overview of quantities and weighting factors for minimization function

3.3 Uncertainty Analysis and Validation

The uncertainties were analyzed to predict the reliability of the calculated orientation. The statistical uncertainties u_{stat} have their origin in uncertainties in the pixel uncertainties described in section 2. The statistical uncertainties in azimuth and elevation are found by means of finite gradients and can be reduced by averaging over *m* facets and *n* pictures. Thus, the statistical uncertainty is reduced by the factor $1/\sqrt{m \cdot n}$.

The components of the systematic uncertainties u_{sys} are the camera (X_0, Y_0, Z_0) and heliostat (X_{Hel}, Y_{Hel}, Z_{Hel}) position as well as facet height W_{Fac} and width H_{Fac}. Variations in focal length have only a negligible sensitivity and are neglected. Figure 3 shows numerically calculated deviations in azimuth (left) and elevation (right). The plotted uncertainty ranges are ±0.5 m for camera and heliostat position, ±1 mm for the facet dimension and ±5 mm for the focal length. In these ranges and for the arbitrarily chosen heliostat (no. 514 of CESA-1 field), camera position, and heliostat orientation (see Table 1), deviations up to 4.7 mrad are observed. The sensitivity of heliostat position is identical to the sensitivity of camera position.

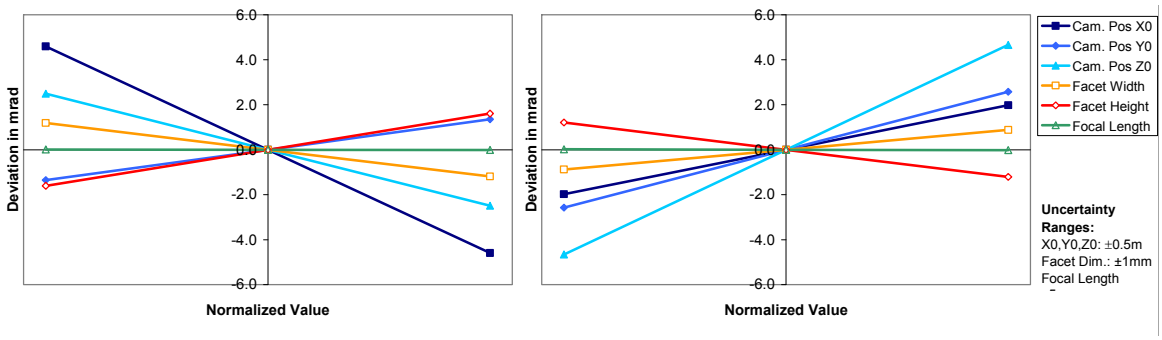

Figure 3. Sensitivity of camera and heliostat position, facet dimensions and focal length to heliostat azimuth (left) and elevation (right). Heliostat no. 514. Details see Table 1

The eight systematic uncertainties are not correlated and partially compensate for each other. The relative combined standard uncertainty in heliostat azimuth results in:

$$\frac{u_c(\alpha)}{\alpha} = \pm\left(\frac{u(\alpha_{sys})}{\alpha} + \frac{1}{\sqrt{m \cdot n}}\frac{u(\alpha_{stat})}{\alpha}\right) \tag{7}$$

Replacing α by β, the identical relations are valid for the heliostat elevation.

A validation of the heliostat orientation measurement system was done at PSA CESA-1 solar tower test facility. For that purpose, the orientation calculated by the previously described method is compared to orientations obtained with flux density measurements. The heliostat was focused on a white target and the actual heliostat aim point was determined by the center of gravity of the beam image.
As the considered sun algorithms differed slightly (maximal 0.5 mrad in the interesting range), the position of the sun is assumed to be the mean value of the algorithms of NREL[6] and DIN 5034 [7]. With this information, the actual heliostat azimuth and elevation can be determined with high accuracy. Figure 4 shows actual and measured heliostat azimuth and elevations over the morning. The plot at the top shows orientation measurements of the heliostat no. 514, the plot at the bottom for no. 506. The two heliostats were chosen due to their different positions in the field: The heliostat no. 506 is located closer to the center and no. 514 closer to the eastern border of the field. For detailed position and orientation data see Table 1. The estimated error bars represent the observed uncertainties very well. All measured heliostat orientations coincide well with the actual orientations within the measurement uncertainty.

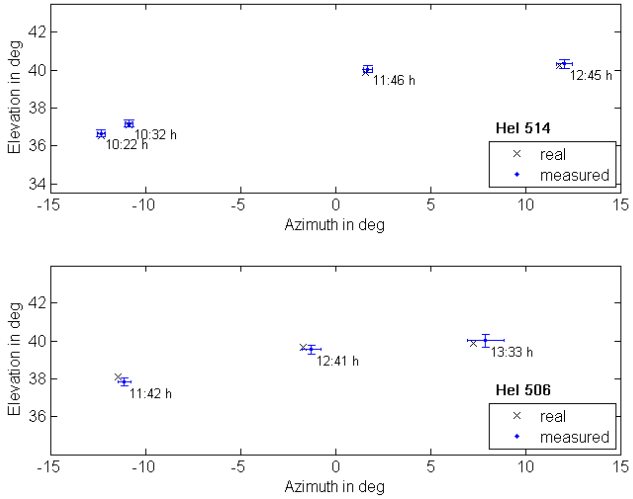

Figure 4. Real and measured heliostat orientation with estimated error. Heliostat 514 (top) and Heliostat 506 (bottom); 24-facet heliostat with averaging over between 2 and 5 images

In Fig. 4 bottom, it can be observed that the measurement uncertainty rises towards solar noon. This is due to the fact that the heliostat normal draws near the camera axis over the morning. Figure 5 shows the uncertainties in heliostat azimuth (left) and elevation (right) for a wide range of orientations. The plots are calculated for a 24-facet CASA heliostat with averaging over five pictures. Further details can be found in Table 3. The behavior of increasing uncertainty with the heliostat normal being parallel to the camera axis is also observed there.

To obtain diagrams independent of heliostat position, the heliostat azimuth and elevation angles are expressed relative to the optical axis of the camera. The resulting diagrams are symmetric to both the elevation and azimuth axis. To find the actual heliostat azimuth and elevation in Figure 5, the camera pan angle must be subtracted from the *x*-values (0° for the chosen CASA-Heliostat) and the camera inclination (measured to the horizontal) must be added to the *y*-values (40.8° for the chosen CASA-Heliostat). Maximum uncertainties are observed if the camera axis is parallel to the heliostat normal. In this case, a small change in heliostat azimuth or elevation hardly influences the corner position in the image. For the chosen heliostat, and orientation (elevation [0°; 80°], azimuth [-60°; 60°]), 50% of the heliostat positions can be measured with an uncertainty below 3 mrad and 80% with an uncertainty below 4 mrad.

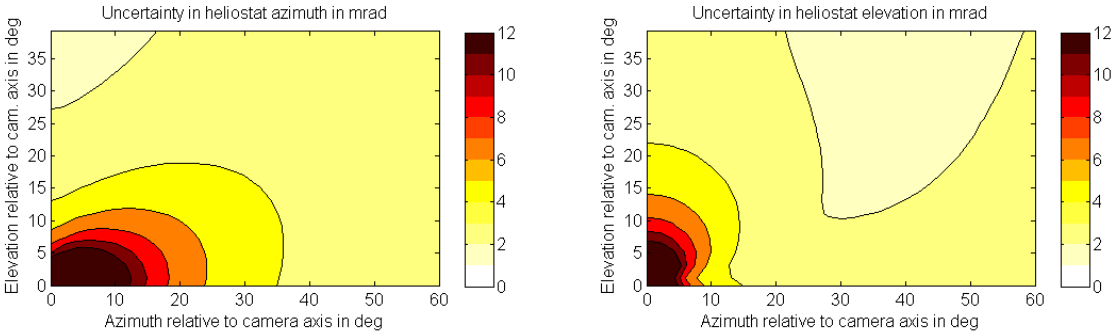

Figure 5. Measurement uncertainty in heliostat azimuth (left) and elevation (right), relative to optical axis of camera (in mrad), for a 24-facet heliostat with averaging over five images

	Value
Camera Position ($X_0/Y_0/Z_0$) in m	(0.0 / 0.0 / 80.0)
Heliostat Position ($X_{Hel}/Y_{Hel}/Z_{Hel}$) in m	(0.0 / 88.0 / 0.1)
Camera inclination (to horizontal) / pan angle	40.8° / 0.0°
Uncertainty in camera position (systematic)	±30 mm in each direction
heliostat position (systematic)	±30 mm in each direction
facet dimensions (systematic)	±1 mm in both directions
corner detection (statistical)	±1 mm in both directions

Origin on tower front side; *x* direction: East; *y* direction: South; z direction: Height

Table 3. Detailed position / orientation data and uncertainties of Fig. 5

4 Photogrammetry

Close-range photogrammetry is a frequently used method to investigate concentrators of solar thermal power plants[1]. This measurement technique uses the information of several images from different perspectives of the same object to evaluate its three-dimensional structure. Heliostats, as well as parabolic through collectors, can be measured with a standard deviation lower than 0.2 mm, providing the possibility to reveal deformations and predict their efficiency. Yet, the preparation and measurement are time-consuming. Retroreflective targets, which can be localized in digital images with high accuracy, must be positioned on the object. The whole measurement procedure, including preparation, data-acquisition and evaluation, takes up to several hours. Here, we present a method which uses the automatically detected heliostat facet corner points instead of the circular-shaped retroreflective targets. The whole procedure works completely automatically, allowing the photogrammetric investigation of one heliostat within 30 minutes. The time saving is, compared to photogrammetry with retroreflective targets, at the expense of accuracy and spatial resolution. Yet, the method is capable to reveal wrongly orientated facets and improve the heliostat canting.

The section starts with a description of the measurement principle. Two approaches to validate the accuracy of this method are made, followed by a comparison of a heliostat structure before and after canting.

4.1 Approach

The investigated object is the CESA-1 heliostat no. 1500 at the PSA with 6x2 facets. To realize the variety of perspectives necessary for a photogrammetric evaluation with a fixed camera position, the heliostat was rotated at two different elevations (30° and 60°) around his vertical axis. The deformation due to the force of gravity between those elevations is below 1 mm. Overall, 98 pictures were taken with a focal length of 460 mm and each

picture was investigated by the edge detection procedure described in section 2. The detected corners were written to a file format readable by the photogrammetry software VMS (Visual Measurement System). The results of the photogrammetric evaluation were available as the three-dimensional coordinates of each facet corner. VMS evaluated a mean precision of 1.2 mm. This value is about a factor ten higher than the accuracy of conventional close-range photogrammetry. One reason for this loss of accuracy is the less exact determination of the corner points compared to retroreflective targets. The accuracy is further decreased by combination of a flat object at great distance together with a zoom-lens, which is atypical for close-range photogrammetry.

4.2 Results and Validation

The results were validated with a conventional photogrammetric measurement (short focal length of 17 mm, fixed object and moving camera, retroreflective targets instead of facet corners) of the same heliostat, which was carried out in a campaign to investigate the gravitational induced deformation of a heliostat for different elevations. Some data processing was necessary to enable the comparison, because the target positions differ from the facet corners (see Figure 1 right). The corrections made imply an additional uncertainty, since the targets were attached with variations of ±3 mm on the mirror plane. However, this has only negligible influence on the accuracy perpendicular to the mirror plane (*z*-direction). For this reason, not only the spatial deviations of the targets were investigated but also the difference of the surface normal between the reference measurement and the results obtained with the edge detection method.

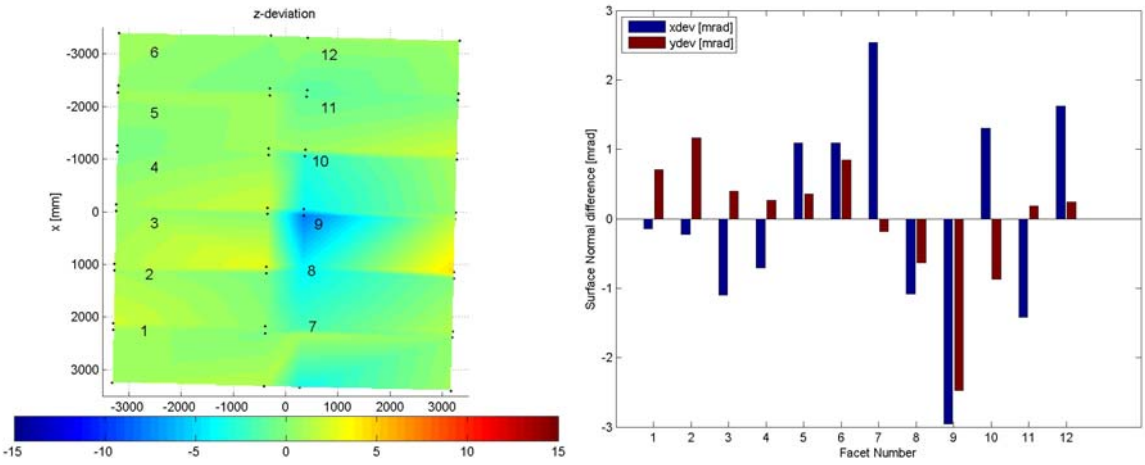

Figure 6. Deviation between new photogrammetric method and conventional reference measurement. Deviations perpendicular to mirror plane in mm, left. Deviations of facet surface normals in mrad, right

In *z*-direction, 98% of the targets have a deviation from the reference measurement of less than 5 mm with a mean deviation of 1.2 mm (see Fig. 6 left). The biggest deviation of 8 mm is found at a corner close to the gearbox. The images used for the edge detection were taken while the targets remained on the mirrors (see Figure 1 right), therefore complicating the edge detection procedure.

The comparison of the normal vectors shows, that all facets except the one with the outlier (facet no 9) have deviations in the range of ±1-2 mrad (see Fig. 6 right). The mean value of the absolute deviations is ±1.6 mrad. This value may be seen as an upper bound for the accuracy of the photogrammetry based on edge detection. Future measurements with improved image quality and without disturbing retroreflective targets remaining on the mirrors are expected to deliver better photogrammetric results. Further validations were not possible because the investigated heliostat was canted shortly after the measurement. However, this offered the possibility to investigate the changes in shape. For this task, the measured surface normals were compared to the ideal parabolic heliostat with a design focal length of 300 meters.

Figure 7 shows the deviations of the surface normals before (left) and after canting (right), revealing the improved performance of the heliostat. Deviations of more than 10 mrad from the desired shape were reduced to values within the current measurement accuracy.

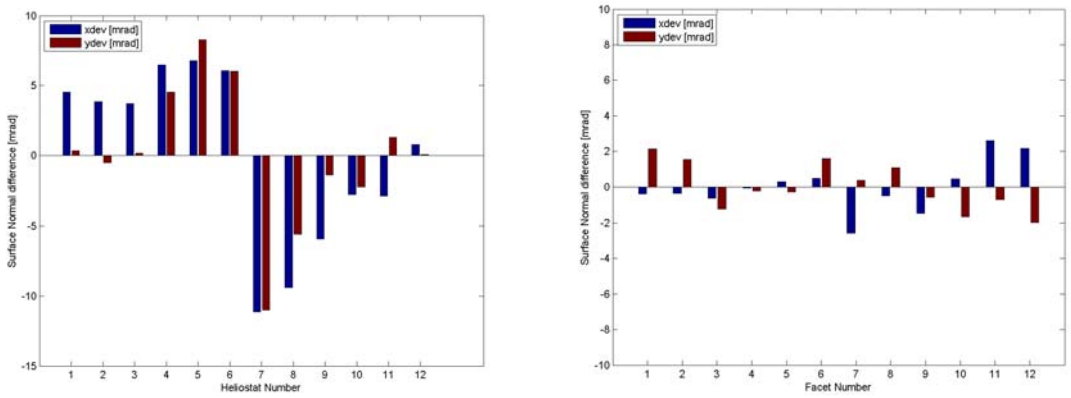

Figure 7. Deviations of facet surface normals from design paraboloid before (left) and after (right) canting

5 Conclusions and Outlook

A fast, cost-effective and automatic characterization tool for heliostats based on edge detection was presented. A digital camera mounted on top of the central receiver tower offers visibility to all heliostats. The pictures are processed automatically and the facet corner image coordinates are extracted. The two presented measurement systems, heliostat orientation and automated photogrammetry, are based on these vertices.

At plant startup, the measurement of the heliostat orientation is helpful to determine drive offsets. During plant operation, an automatic monitoring of the heliostat tracking improves efficiency. It was shown that the new heliostat orientation tool can measure heliostat orientations in 50% of the cases with an uncertainty below 3 mrad and in 80% of the cases with an uncertainty below 4 mrad. This is assessed to be sufficient to detect wrongly tracking heliostats. The results are available approximately three minutes after taking the pictures. Further investigations to enhance accuracy are planned.

A second application of the corner detection is to apply the automatically extracted data to photogrammetry without the time-consuming manual application of retroreflective targets. A set of pictures is taken from the camera located on top of the tower while the heliostat moves. Then, the heliostat shape can be measured by means of photogrammetric methods. Manual close-range photogrammetry with mounted retroreflective targets is still the method of choice to study the deformation and structure of single heliostat prototypes. In contrast, the presented new photogrammetry method by edge detection is much faster (approximately 30 minutes) and completely automatic but with the price of lower accuracy. Its application is therefore the general inspection of the canting condition of entire heliostat fields. It was demonstrated that the achieved accuracy for the facet normal vectors is approximately 1.6 mrad for the investigated heliostats. Hence, major facet misalignments in an existing heliostat field can be detected economically in this way.

Acknowledgements

Financial support from the German Federal Ministry for the Environment, Nature Conservation and Nuclear Safety (Saphir Contract 16UM0068) is gratefully acknowledged.

References

[1] Pottler, K.; Lüpfert, E.; Johnston, G.; Shortis, M.: A powerful tool for geometric analysis of solar concentrators and their components, Journal of Solar Energy Engineering 127, pp. 94-101, 2005.

[2] Ulmer, S.; Röger, M.: Automatisierte hochaufgelöste Vermessung der Spiegelfehler von Heliostaten. In: 10. Kölner Sonnenkolloquium, Deutsches Zentrum für Luft- und Raumfahrt (DLR) e.V., Köln, 21. Juni, 2007.

[3] Gonzales, R.; Woods, R.; Eddins, S.: Digital Image Processing using Matlab, Pearson, 2004.

[4] Houck, Christopher R.; Joines, Jeffery A.; Kay, Michael G.: A Genetic Algorithm for Function Optimization: A Matlab Implementation, North Carolina State University, Raleigh, NC, NCSU-IE-TR-95-09, 2005.

[5] Lagarias, J.C., Reeds, J. A.; Wright M. H.; Wright, M. H.: Convergence Properties of the Nelder-Mead Simplex Method in Low Dimensions, SIAM Journal of Optimization, Vol. 9 Number 1, pp. 112-147, 1998.

[6] Reda, Ibrahim; Afshin, Andreas: Solar Position Algorithm for Solar Radiation Applications, National Renewable Energy Laboratory, Golden, CO, NREL/TP-560-34302, Revised Version, Nov. 2005.

[7] DIN 5034 Teil 2: Tageslicht in Innenräumen; Grundlagen, Deutsches Institut für Normung, Berlin, Beuth Verlag, Köln, 1985.